

Magnetic reconnection: a common origin for flares and AR interconnecting arcs

L.G. Bagalá¹, C.H. Mandrini², M.G. Rovira², and P. Démoulin³

¹ Max Planck Institut für extraterrestrische Physik, Postfach 1312, 85741 Garching, Germany

² Instituto de Astronomía y Física del Espacio, IAFE, CC.67, Suc. 28, 1428 Buenos Aires, Argentina

³ Observatoire de Paris, DASOP, URA 2080 (CNRS), 92195 Meudon Cédex, France

Received 2 August 2000 / Accepted 22 September 2000

Abstract. We present a study of active region (AR) 7031, where several flares occurred throughout the last week of January, 1992. We analyze in detail the three largest flares, both in H α and soft X-rays. During its transit across the disk this region interacted with another one (AR 7038), as indicated by the recurrent brightening in soft X-rays of an interconnecting loop, accompanied by sympathetic flaring.

Using a linear force free extrapolation of the photospheric magnetic field, we compute the locations of Quasi-Separatrix Layers (QSLs), which are the likely places where the magnetic field can reconnect. We find that flare brightenings can be linked by field lines having footpoints at the QSLs. Furthermore, field lines connecting AR 7031 and AR 7038 belong to the QSLs computed when magnetograms from both ARs are combined. We conclude that both soft X-ray flare loops and interconnecting loops result from magnetic reconnection at the QSLs. Which of the many QSLs found in the computations are the site of magnetic reconnection depends on the magnetic field evolution. In the studied ARs we can identify three different drivers for energy release: flux emergence, photospheric displacements of the polarities and nearby magnetic reconnection. This last process leads to sympathetic flaring and to the brightness enhancement of the interconnecting arc.

Key words: methods: data analysis – Sun: flares – Sun: magnetic fields

1. Introduction

The old debate about how many loops are involved in a flare appears to have no end. The main reason is because there are roughly as many observed flaring configurations in soft X-rays having one loop as having a multiple loop structure. After the first results from the Soft X-ray Telescope (SXT, Tsuneta et al. 1991) the configuration with one single loop and two footpoints in soft X-rays became more popular (Dennis et al. 1994), but at the same time the evidence for flares with interacting multiple

loops (Hanaoka 1996; Yoshida & Tsuneta 1996; Liu et al. 1998) and with multiple sources in hard X-rays (Sakao et al. 1994) has increased as well.

Khodachenko and Zaitsev (1998) modeled energetic processes in solar ARs. They concluded that energetic processes in individual magnetic loops lead to a flare-like heating of nearby loops. That means, a multiple loop structure is considered. Hori et al. (1998) used hydrodynamic simulations to reproduce spectral profiles observed in the early phase of solar flares. They found that only multiple-loop systems are compatible with their models. In Démoulin et al. (1997) the authors show that in all the flares they have studied more than one single loop is involved. Ozaki et al. (1997) studied by means of a three-dimensional magneto-hydrodynamic simulation the interaction of magnetic loops and arcades. They found that a single loop or arcade does not exhibit any significant energy release, even though it is highly twisted and expanded. These authors also concluded that a flare-like energy release can occur only when two flux tubes collide and reconnect with each other.

The idea of energy release in flares driven by reconnection in separatrixes is intimately related with a multiple-loop structure. In separatrixes, the field-line linkage is discontinuous. There, field lines can reconnect and the magnetic field can relax to a new, less energetic configuration. The generalization of the concept of separatrixes to configurations without field-line linkage discontinuities was put forward by Priest & Démoulin (1995). They proposed that magnetic reconnection may occur in 3D in the absence of null points at “quasi-separatrix layers” (QSLs), which are regions where there is a steep gradient or a drastic change in the mapping of field lines from one boundary to another of a given magnetic volume. They proved that in a special configuration (a sheared X-type magnetic field), nearly any smooth and weak flow imposed on the boundary produces strong flows at the QSLs. Démoulin et al. (1996) have determined the location of QSLs and studied their properties in simple theoretical flaring configurations. To do that, they have developed a numerical algorithm called QSLM, for Quasi-Separatrix Layers Method. Their results have been extended successfully to observed configurations (e.g. Démoulin et al. 1997; Mandrini et al. 1997; Schmieder et al. 1997; Gaizauskas et al. 1998).

Send offprint requests to: L.G. Bagalá (gbagala@mpe.mpg.de)

Large-scale structures in the solar corona have been observed since 1970, starting with the Skylab X-ray instrument, only in soft X-rays. These early observations had a poor temporal resolution (see e.g. Chase et al. 1976; Fárník & Svestka 1986), but nevertheless, more than a hundred interconnecting loops were observed. HXIS (on board the Solar Maximum Mission), with better timing but poorer spatial resolution, has also observed interacting ARs connected through a large scale arc (De Jager & Svestka 1985; Poletto et al. 1993). Howard & Svestka (1977) and Svestka & Howard (1979, 1981), studying Skylab data, concluded that brightness variations of the loops are always caused by magnetic field changes near their foot-points. These changes can also produce flares in the connected regions, but the flare occurrence and the loop brightenings are independent consequences of one common trigger action (e.g. the emergence of a new bipole). SXT, on board the Yohkoh satellite, has better temporal and spatial resolutions. At present, over 100 interconnecting loops measured with SXT have been analyzed. The first results (Manoharan et al. 1996; Tsuneta 1996; Pevtsov et al. 1996; Fárník et al. 1999) suggest strongly that magnetic reconnection is the trigger for the development and/or the brightening of the interconnecting loops. Several studies proposed also that different loops can interact in such a way that an instability in one loop system can be transmitted to another loop system rooted nearby (Rompolt & Svestka 1996). The example described here suggests that both possibilities are present at different times.

We study the magnetic evolution of AR 7031 throughout a week, and compare this evolution with the location of flare emission in $H\alpha$ and soft X-rays. As we have observed the brightening of a loop connecting AR 7031 to AR 7038, we have analyzed this arc and we have generated a magnetogram combining the two ARs. The magnetic field evolution is described in Sect. 2. The flare data are analyzed in Sect. 3. After this, we show the results of the magnetic field model and of the computed topology for the studied regions, and compare the location of QSLs to observed features (Sect. 4). We conclude, first that energy is released by magnetic reconnection, and second that the magnetic evolution (e.g. emergence of flux, displacement of the photospheric polarities and changes in the configuration due to nearby magnetic reconnection) is what determines the location of the energy release sites at QSLs for the flares and the interconnecting arc (Sect. 5).

2. Magnetic field data

2.1. The magnetic evolution of AR 7031

AR 7031 traversed the solar disk during the last week of January and the first week of February, 1992. Mees Solar Observatory (MSO) obtained the magnetic data using the Mees Stokes Polarimeter (Mickey 1985). On January 30, the day in which the three most important flares happened, the AR was located at S07 W06 on the solar disk.

In Fig. 1 we present the magnetogram rasters corresponding to January 28, 29, 30 and 31, 1992. The time identification is the starting time of the raster, although the scan took up to 3

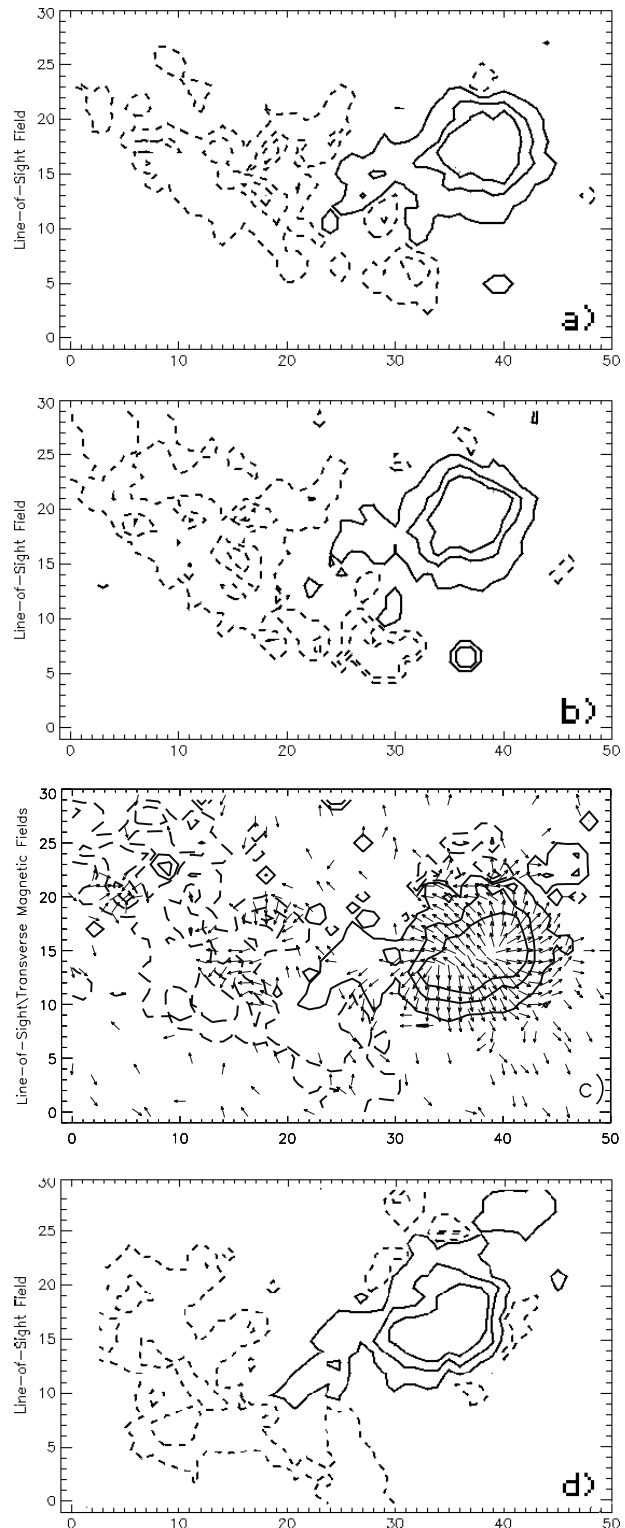


Fig. 1a–d. Longitudinal magnetograms corresponding to AR 7031 on **a** January 28 (22:17 UT); **b** January 29 (01:48 UT); **c** January 30 (18:06 UT) and **d** January 31 (18:54 UT), 1992. Full (dashed) lines represent positive (negative) values of $\pm 100, 500, 1000$ G. The axes are expressed in magnetogram pixels. In **c** we show the transverse magnetic field above 200 G, the length of the arrows is proportional to the logarithmic value of the field intensity. In this figure and in Fig. 2, terrestrial North is up and West is to the right.

hours to complete a full magnetogram. The line measured in this opportunity was Fe I (λ 6301). The spatial resolution was 5.7", covering a field of view (FOV) of ($5' \times 7'$). The highest spatial resolution magnetograms (2.8"), were obtained for single spots only, so we have used them to visualize some morphological details in smaller areas of the AR, and the direction of the transverse field.

AR 7031 is mainly bipolar (see Fig. 1), with a positive and very concentrated preceding spot and a diffuse and more extended following polarity. The strongest positive longitudinal region remained almost unchanged during these days, while some new positive flux was seen emerging in the weakest field region towards the East of the main spot. The negative region underwent several modifications. Negative magnetic flux emerged towards the South between January 28 and 29, and also towards the East between January 29 and 30. By January 31, the negative flux in the southeastern portion of the AR had started to decrease. On the other hand, a new bipole started to emerge at the North of the main positive spot on the 28 and is clearly seen on the 30 and 31. The transverse field (see Fig. 1c) looks in general potential. However, there are two localized zones of non-negligible shear related to the events studied in this paper; these are: a) the eastern portion of the longitudinal inversion line between the main positive and negative polarities and b) the longitudinal inversion line between the new bipole negative polarity and the main positive spot. The vertical current density, obtained from the observed transverse field, is above 10 mA/m^2 only at the location named in b). At the place named in a), the transverse field is too low to obtain reliable current density measurements; in this case the presence of shear in the field is mainly indicated by the direction of the $H\alpha$ fibrils.

2.2. The combined magnetic field of AR 7031 and 7038

We have found in the SXT largest FOV an interconnection arc linking AR 7031 with another region (AR 7038) (see Sect. 3.2.2). We then use the full-disk longitudinal magnetograms obtained with the Vacuum Telescope at Kitt Peak National Observatory (KPNO, Livingston et al. 1976), in which both ARs can be observed. However, the values of the field in regions where $B_l > 1000 \text{ G}$ are uncertain in KPNO magnetic maps, probably due to a problem of stray light in the telescope (Harvey J., private communication); for that reason, we have used the MSO magnetograms in our study, although none of the magnetograms have both ARs in their field of view. MSO took a magnetogram of AR 7038 on January 30 at 21:54 UT. AR 7038 is a bipolar region smaller and with a lower intensity field than AR 7031. In this magnetogram we observe an important departure from potentiality but, as the field intensity is low, the transverse field measurements are hardly above the noise level.

As we intend to compare the location of the interconnection arc with the topological structures of the field (see Sect. 4), we have to combine both ARs in the same map. To do so we have to take into account: a) the relative location of the ARs (for this purpose the magnetogram of KPNO was used), b) the differential rotation of the Sun since both ARs were located at

different latitudes, c) the time and the time interval during which the magnetograms were taken. This last point is the issue because, although we know the starting time of the observation, the magnetograph took more than 2 hours to scan each complete field. AR 7031 was located at S07W06 and AR 7038 at S12W17. The magnetograph scans the field following a zig-zag path, beginning with a pixel at the North East. Taking this into account, and considering the total duration of the scan, we can estimate the time when the southwestest pixel of the northern region (AR 7031) was taken. After that, we corrected by differential rotation and we found in this way the coordinates (latitude and longitude) of the nearest pixels of both regions. As in the full disk KPNO magnetogram the ARs appeared isolated and surrounded by very low field concentrations, we created a matrix where both ARs were placed at their "true" locations and we filled with 0 G the pixels without measurements (Fig. 4d).

3. The events in the complex AR 7031 – AR 7038

3.1. An overview

Concerning the flare activity, AR 7031 was clearly more important than AR 7038. AR 7031 produced 12 flares, classified as type C or higher in soft X-rays, between January 27 and 31, 1992, and several weakest flares and subflares (Solar Geophysical Data, SGD 575 Part II). SXT observed almost all the flares that occurred in this region, and the Mees CCD Imaging Spectrograph (MCCD, Penn et al. 1991) at MSO recorded their $H\alpha$ emission.

The loop that connects AR 7031 and AR 7038 was bright in soft X-rays at least since its appearance on the disk, on January 24, 1992. By that date no bright plage was seen in $H\alpha$ at the location of AR 7038, while at photospheric level a bipolar flux concentration of very low intensity was observed indicating the growing stage of AR 7038. AR 7038 was reported as a new active region just on January 27. From then on, the new AR started to flare weakly. Between January 28 and 30, 1992, AR 7038 produced 18 subflares and an $H\alpha$ 1F flare on January 29, 13:25 UT. Simultaneously, the emission of the interconnection arc increased. Two sympathetic subflares occurred in AR 7031 around that time, one before (at 13:18 UT) and one after (at 13:28 UT) the 1F flare in AR 7038.

3.2. The flares on January 30, 1992

The 3 most intense flares in the analyzed period were observed on January 30 in AR 7031, at 02:23 UT (classified 2N in $H\alpha$ and M 1.6 in X-rays), 09:35 UT (classified 2B and M 4.9) and at 19:35 UT (classified as 2B and M 2.4). The first two were homologous, but the other one did not happen in the same zone of the AR. We describe here the evolution of these flares using SXT data and $H\alpha$ data from MCCD.

To co-align the data in different wavelengths we have used the sunspots for corregistration. SXT provided, at that time, white-light images through the narrow-band filter, the MCCD images include both the line and the continuous flux, while the magnetograph data allow us to relate higher values of the

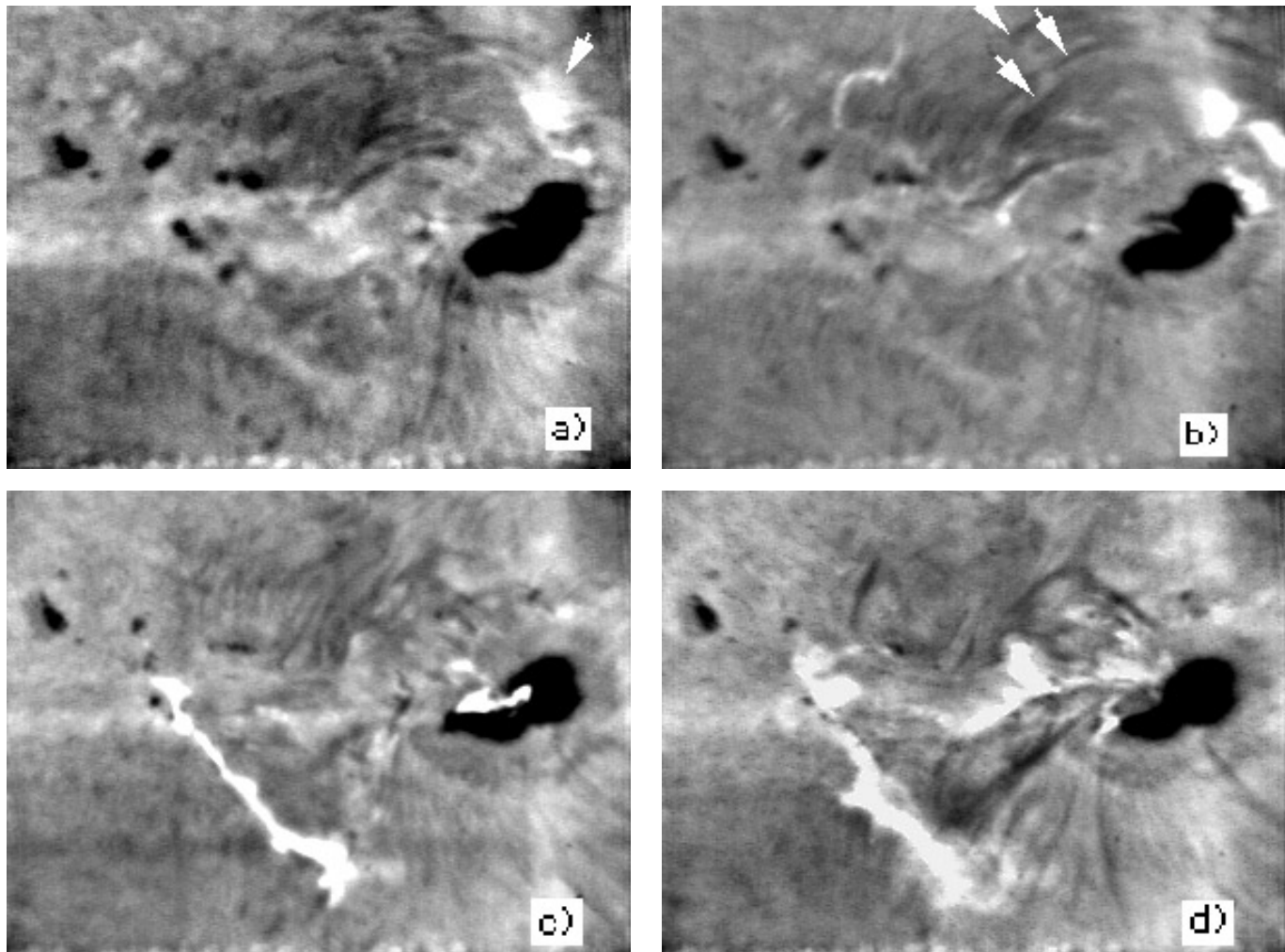


Fig. 2a–d. Emission in $H\alpha$ for the flares **A** and **B** on January 30, 1992. **a** and **b** Flare **A** at 02:22 UT and at 02:37 UT, respectively. **c** and **d** Flare **B** at 19:44 UT and 20:44 UT, respectively. In **a** the arrow points to the place where we observe the $H\alpha$ emission expanding towards the North East, while in **b** they point to the long $H\alpha$ loops (which extend partially out of the observed frame).

longitudinal field with white-light spots. Taking a conservative approach, we consider that the overlays among SXT, MCCD and magnetic data are accurate to $\approx \pm 6''$.

3.2.1. The data in $H\alpha$

The $H\alpha$ data have been analyzed using mainly co-aligned movies. In Figs. 2 we can see $H\alpha$ images for the main flares on January 30, 1992. For comparison, the preceding spot (positive) can easily be superimposed with the main positive polarity in Fig. 1c. The emission for the flare at 02:23 UT, to which from now on we will call “**A**”, starts at the North of the preceding spot over the inversion line between the small negative and positive flux concentrations (see Fig. 1c). Almost all the flares in this AR started at this place. MCCD shows some very elongated $H\alpha$ dark fibrils extending from East to West in the northern portion of the AR prior to the flare onset. This orientation is coherent with the observed transverse field and indicates the presence of magnetic shear in the AR. As the flare evolved, the emission,

first localized, expands towards the North and it goes out of the MCCD field of view (see e.g. Fig. 2a). We observe that material flows towards the North East starting probably at the same place where the flare erupted. The trajectory followed by this material agrees with the shape of an arcade observed in soft X-rays (see next section). During the main phase, dark elongated loops are seen at the North of two main polarities (pointed by arrows in Fig. 2b). The flare at 09:35 UT, to which from now on we will call “**A'**”, evolves in a similar way, although we don't observe the same expansion of the $H\alpha$ emission.

The two-ribbon flare at 19:35 UT, that we will call “**B**” started emitting in a very elongated band, following the shape of the main eastern inversion line, and a shorter one, located almost over the positive spot (Fig. 2c). After the impulsive phase, the eastern band widened and extended; while the western one seemed to rotate counter clockwise and evolved into an elongated brightening very close to the inversion line at the North East of the main positive polarity (Fig. 2d).

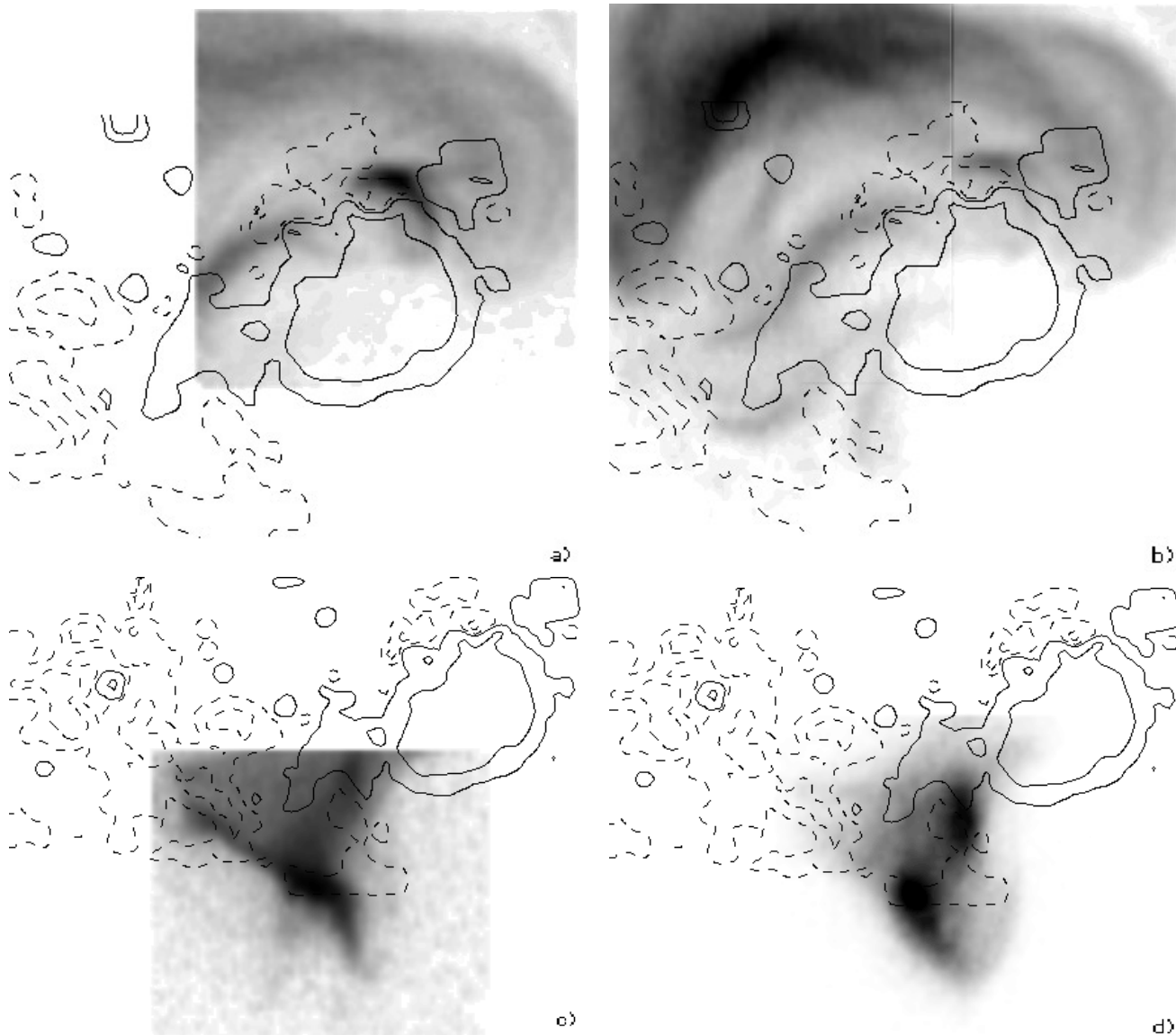


Fig. 3a–d. Soft X-ray (negative) images using the A112 filter and the best resolution of SXT: **a** flare **A'** at 09:50 UT; **b** flare **A'** as a composition of two images recorded at 09:55 and 10:00 UT; **c** flare **B** at 19:47 UT; **d** flare **B** at 20:04 UT. The longitudinal magnetogram on January 30 (contours of ± 100 , 500 G) has been superimposed. In these and the following figures heliographic North is up and West is to the right.

3.2.2. The data in soft X-rays

We have used the SXT data to investigate the morphology of the hot flaring plasma. Images were taken in the four SXT filters: A10.1, AlMg, A112 and Be119, listed in increasing order of energies. The response of these filters lies in the range 1–2 keV. During the three flares, images were taken both in flare and quiet mode and in the three different available resolutions. Images shown in Figs. 3 were taken using the best resolution (2.5'') provided by the instrument and the smaller FOV (64×64 pixels in size). In these figures the magnetogram obtained on January 30 has been superimposed.

The soft X-ray emission from flares **A** and **A'** is concentrated in the same zone as the $H\alpha$ brightenings. It started on the same portion of the inversion line between the small negative and positive flux concentrations, at the North of the main positive

polarity (Fig. 3a). As the flares evolved, the initial brightening splitted in two and we can also see a large arcade with the same orientation of the dark $H\alpha$ loops, clearly connecting this zone with the northeastern portion of the main negative polarity (Fig. 3b). The difference between flare **A** and **A'** is that in **A** we can see the arcade emitting faintly, while in **A'** it is as bright as the main flaring kernel.

Flare **B** starts with a single intense brightening at the South East of the positive spot (Fig. 3c); as the flare evolves, we observe two nuclei (Fig. 3d) probably corresponding to the foot-points of a set of loops. Fig. 4 shows a temporal sequence of SXT images for flare **B** in the A10.1 filter at quarter resolution (9.8''). The total FOV is the largest provided by the SXT partial frame (covering four times the smallest FOV). We see that when the emission reaches its maximum another zone, where AR 7038

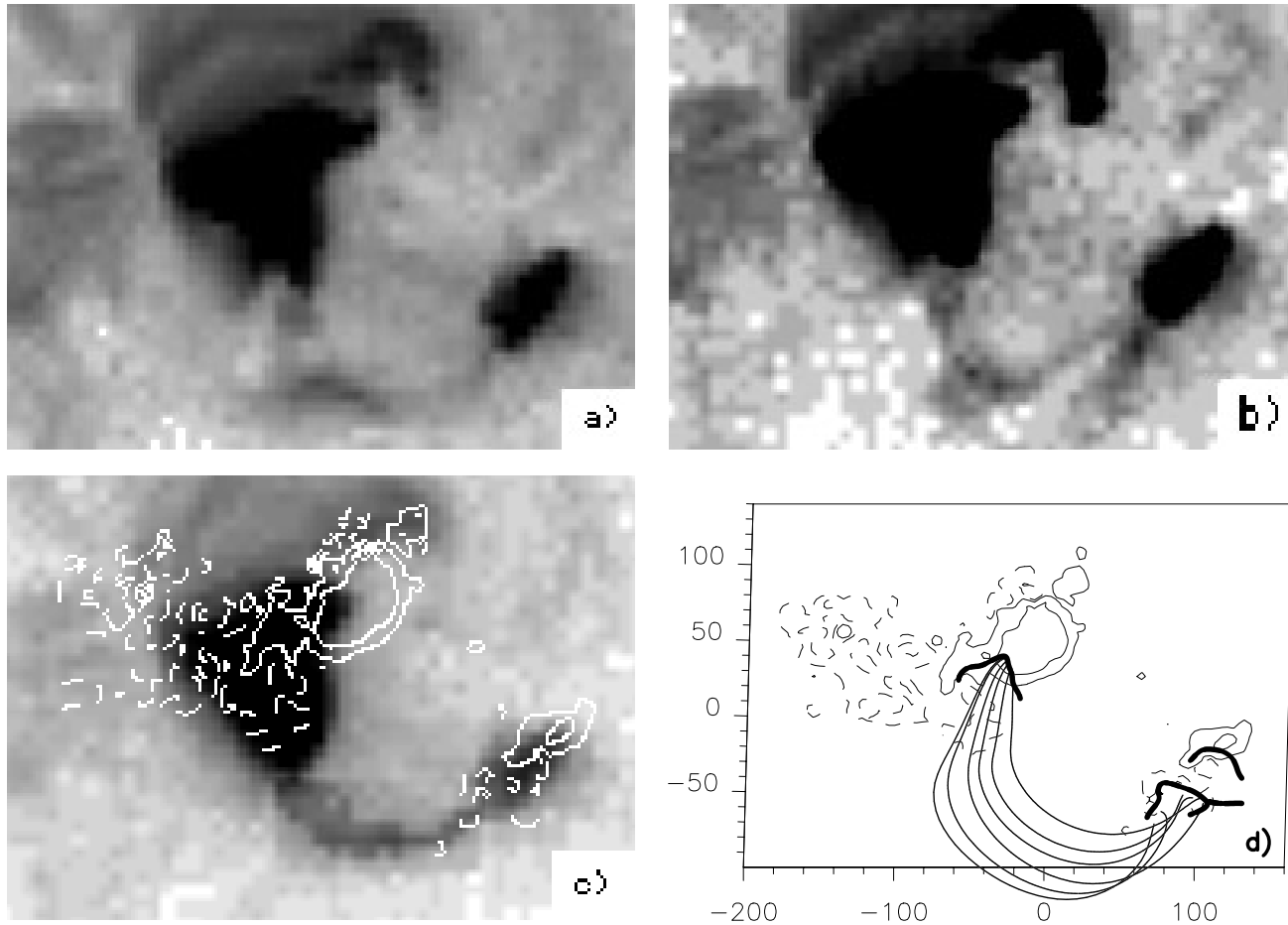


Fig. 4a–d. Temporary sequence of SXT images (largest FOV in A10.1) for flare **B** at: 19:46 UT (**a**), 19:50 UT (**b**) and 20:06 UT (**c**). The flare appears saturated so the much fainter arc can be observed. **d** corresponds to the magnetic field model of the combined regions. Some field lines following the shape of the interconnecting arc have been added. These lines have their footpoints at the computed QSLs (see text), which are shown at photospheric level as thick continuous lines. The isocontour values of B_l are $\pm 100, 500$ G. The box axes are labelled in Mm.

is located, emits in sympathy with AR 7031. The interconnection arc is clearly seen connecting both ARs. This arc was far from being quiet, we first identify a bright loop, as shown in Fig. 4a at 19:46 UT. As the time proceeds, the emission seems to bend towards the South and afterwards we can identify several independent loops (Fig. 4b). The northwestern zone of AR 7031, where flares **A** and **A'** developed, was also seen emitting in X-rays. From this time, and until 19:56 UT, all SXT images are saturated. In Fig. 4c, the loop is again observed having the shape it had before the flare.

4. The magnetic topology of the complex AR 7031 – AR 7038

4.1. The magnetic field model

The photospheric longitudinal field (B_l) has been extrapolated to the corona, under the linear force-free field assumption ($\nabla \times \mathbf{B} = \alpha \mathbf{B}$, with constant α), using the discrete fast Fourier transform (FFT) method as proposed by Alissandrakis (1981). The main limitations of our extrapolation method are: imposed

flux balance, periodicity of the solution in the horizontal (x, y) directions, proportionality between the current density and the magnetic field (through the constant α).

We have modeled the magnetic field using as boundary condition the line of sight component of the map built combining both regions on January 30, 1992. In our model we take into account the projection effects due to the location of the ARs on the solar disc, as described in Démoulin et al. (1997). Using a linear force-free model for the field, we are not able to fit locally the transverse field measurements (the higher transverse field regions are too localized, as mentioned in Sect. 2.1). We have determined a global value of α by comparing computed field lines with the best observed SXT loops during the flares. This value turned out to be $\alpha = 0.009 \text{ Mm}^{-1}$. The model of the field is shown in Fig. 5. Notice also, that the direction of the computed field lines at low heights agrees well with the direction of the observed transverse field. However, in order to fit the shape of the interconnection arc it was necessary to increase the value of α to 0.014 Mm^{-1} . The resulting model is shown in Fig. 4d. The coronal magnetic field is most probably non-linear force free;

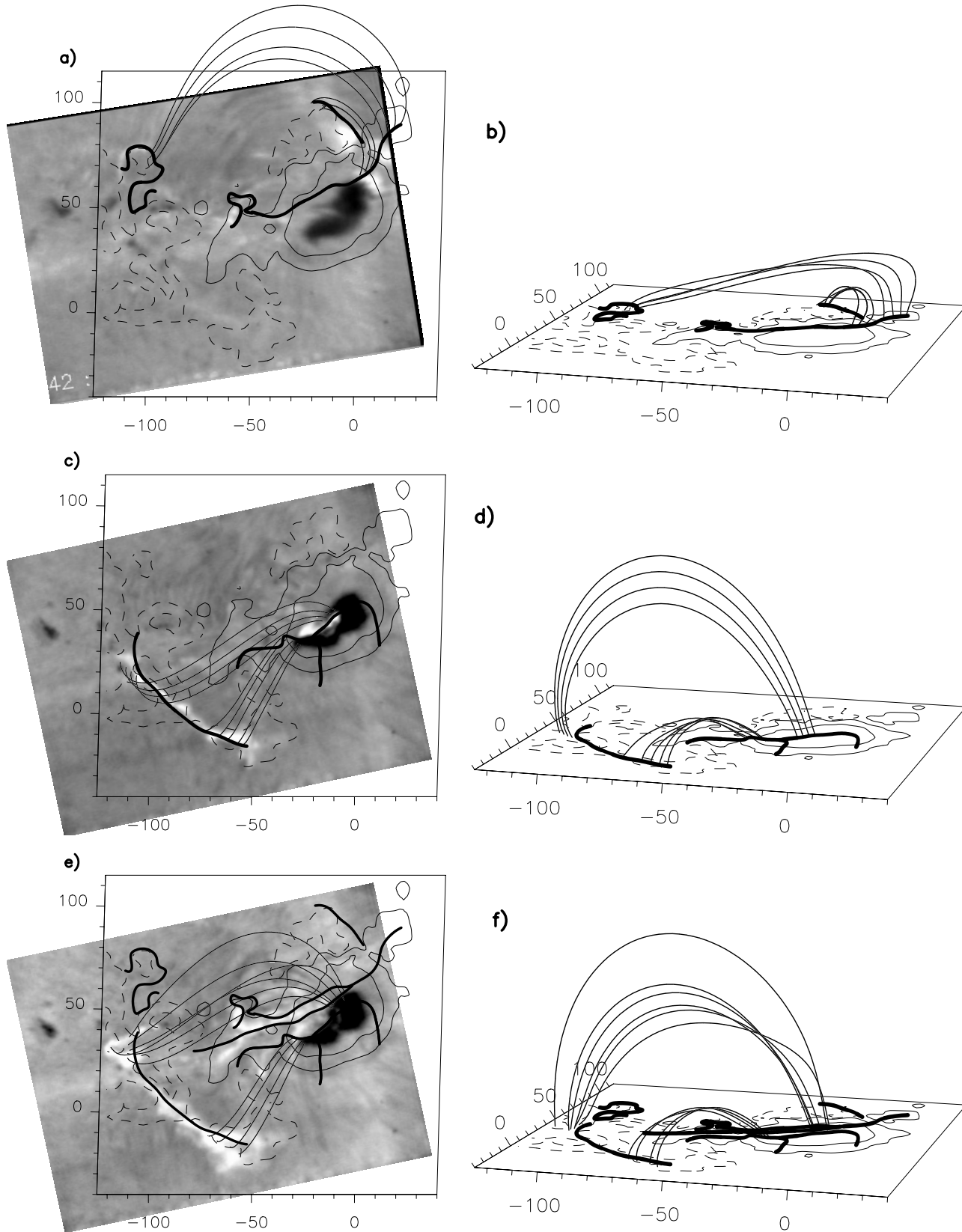


Fig. 5a–f. Magnetic model and topology of the magnetic field of AR 7031. We have drawn sets of computed field lines that follow the shape of the soft X-ray loops and that have their footpoints at both sides of the QSLs, where the $H\alpha$ brightenings are located. **a** and **b** correspond to flare **A**; while **c–f** correspond to flare **B** (see text). The magnetic field isocontours are the same as in Fig. 4. The box axes are in Mm and the photospheric locations of QSLs are shown with thick continuous lines.

therefore, this higher value of α should be related to the high localized magnetic shear observed in AR 7038.

4.2. QSLs and their relation with the observed events

Following Démoulin et al. (1997), we use here the QSLM to find the locations of QSLs and analyze their relation to the observed flares. QSLs are regions where field lines initially close together separate widely when we follow them. QSLs are defined in terms of a dimensionless function N , which is:

$$N(x, y) = \sqrt{\sum_{i=1,2} \left[\left(\frac{\partial X_i}{\partial x} \right)^2 + \left(\frac{\partial X_i}{\partial y} \right)^2 \right]}. \quad (1)$$

being $X_i = x''_i - x'_i$, x'_i and x''_i the photospheric footpoints of a given field line; while x, y are the coordinates along the photospheric plane which lies at $z = 0$. The locations where $N(x, y)$ takes its highest values define the field lines involved in the QSLs. We refer the reader to Démoulin et al. (1996) for a discussion of the properties of $N(x, y)$ and of the basic characteristics of QSLs. Applications of the QSLM to different observed phenomena can be found in Mandrini et al. (1996), Schmieder et al. (1997), Démoulin et al. (1997) and Gaizauskas et al. (1998).

AR 7031 is essentially a bipolar region, except for the several small flux concentrations that emerged between January 29 and 30; in particular the small bipole at the North of the main positive polarity. The topology of the field is complex since the flux of the very intense preceding polarity is shared by all the surrounding negative fields. In Figs. 5 we show the locations of the QSLs computed for the magnetic field model of the combined ARs. For the sake of clearness, we have drawn in Fig. 5a–b the QSLs associated to the flares **A–A'** (which we will call the northern QSLs), and in Fig. 5c–d those associated to flare **B** (which we will call the southern QSLs). In Fig. 5e–f we have combined both sets of QSLs together with a central one to where the $H\alpha$ emission of flare **B** extends during its late phase. The location of flare brightenings in $H\alpha$ agrees with the intersection of the QSLs with the photosphere for all the observed flares.

According to the evolution of the flares described in Sect. 3, we see that the magnetic structures associated to the northern QSLs do not interact with the ones related to the southern QSLs during flares **A** and **A'**; no brightenings are observed either in $H\alpha$ or soft X-rays related to field lines having their footpoints at the southern QSLs. However, during flare **B** soft X-ray emission is observed (see Fig. 4c) following the shape of field lines related to the northern QSLs (see Figs. 5a–b). This implies that during this large event energy release occurring at one site of the AR might induced energy release at a different one. We now discuss the different events in particular.

4.3. Emerging bipole: flares **A** and **A'**

The homologous flares **A** and **A'** occurred in a recurrent flaring place for AR 7031. In Figs. 5a–b we have drawn sets of field lines with footpoints lying at both sides of the photospheric portion

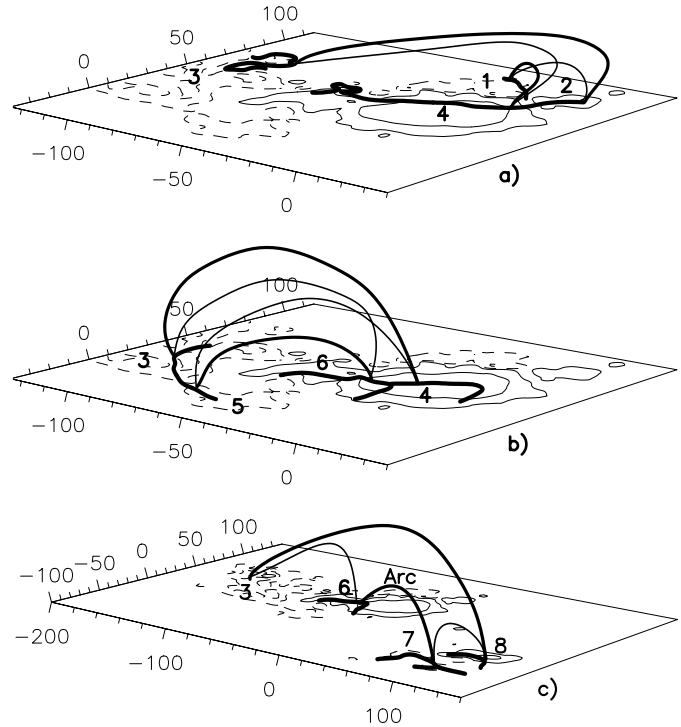


Fig. 6a–c. Magnetic connectivities and interacting bipoles. **a**, **b** and **c** outline the connectivities before/after (thin/thick continuous coronal lines) magnetic reconnection for flares **A–A'**, **B** and the interconnecting arc, respectively. The numbers in the figures indicate which are the interacting polarities in each case. The field line sketch is drawn on the photospheric field model where we have also included the locations of QSLs (thicker continuous lines), the convention for the field and spatial dimensions are the same as in Fig. 5.

of QSLs. These field lines are formed by magnetic reconnection at the QSLs during flares **A** and **A'**. The magnetic connectivity, before reconnection occurs, corresponds to the link between the positive and negative field in the main large bipole and in the small emerging bipole (the four kinds of connectivities and the two interacting bipoles are shown in Fig. 6a). Notice that the set of reconnected field lines (see Fig. 5a–b) clearly follows the shape of the soft X-ray arcade connecting the big preceding positive polarity to the northern portion of the following elongated negative polarity (Fig. 3a–b).

Three bright kernels can be seen in Fig. 2b, while a fourth fainter brightening is seen at the footpoints of the field lines fitting the shape of the soft X-ray arcade. This very faint kernel can be observed only in a few images of the set corresponding to both flares (**A** and **A'**) and it can be easily over-seen when looking at the movies. However, since it is located on the QSL lying on the following polarity, and its shape matches the shape of that portion of the QSL, we were able to find it using the topology of the magnetic field let us locate a faint brightening not visible at first sight in the flare data (Bagalá et al. 1995).

Summarizing, we conclude that the emergence of the north-western bipole lead to the interaction between loops associated

to it with the northern loops belonging to the AR main bipolar field. This interaction was the origin of **A** and **A'** flares.

4.4. Bipolar configuration: flare **B**

Flare **B** is a two-ribbon event. In this case the brightenings are located on the southern QSLs. In Figs. 5c and d we show sets of reconnected field lines having footpoints at both sides of the QSLs at the place of the $H\alpha$ ribbons. The topology of the field related to this event is typical of bipolar configurations, where two elongated QSLs are found; however, two sets of interacting field lines can be identified as in a quadrupolar field (Démoulin et al. 1996). Fig. 6b illustrates the connectivities before and after reconnection and identifies the polarities of the interacting bipoles. We suggest that the evolution of the following polarity (compare Fig. 1b–c) induces the interaction between the magnetic structures associated to the southern QSLs. Energy release occurring at the QSLs is the origin of flare **B**. As the flare evolves (see Figs. 2c–d), the ribbons expand but they still lie close to QSLs. Notice that the originally more concentrated ribbon extends towards a portion of a different QSL at the North during the gradual phase of the flare (see Fig. 5e–f). This implies that close by magnetic structures become involved in the energy release process as discussed in Sect. 5.

4.5. Interaction between ARs: interconnecting arc

Concerning the large scale interconnection arc, Fig. 4 shows that field lines, issued from some of the QSLs lying on the main positive polarity, extend towards AR 7038. These field lines match the shape of the arc, as observed during the occurrence of flare **B**, and have their opposite footpoints at the QSLs located on the negative polarity in AR 7038. These results let us conclude that energy release at the QSLs, associated with AR 7031, produces the enhancement of the interconnection arc and may induce the occurrence of flares in AR 7038 (see Sect. 3.1).

What is the physical origin of the interconnecting arc? Compared to flares **A**, **A'** and **B**, the observations of the arc are much less proving since the changes induced in the atmospheric plasma after energy release are less evident (e.g. no significant $H\alpha$ brightenings and a low soft X-ray emissivity). Nevertheless, the topology shown in Fig. 4d, together with the theoretical knowledge of the magnetohydrodynamic evolution of two interacting bipoles, let us propose the following scenario. First, free magnetic energy is present in both regions, as indicated by the transverse magnetic field, and also probably a current layer develops between the two ARs (formed by the interaction of the two initially independent configurations represented in Fig. 6c by the two thin lines). The relative slow evolution of the ARs (in particular the rotation of AR 7038) is expected to induce a low reconnection rate between sets of loops belonging to them. This is probably the origin of the weak interconnecting arc seen before flare **B**. During flare **B**, fast modifications in the field of AR 7031 induce a higher reconnection rate. In both cases, reconnection is forced by the magnetic evolution of the individual ARs. The multi-loop system forming the interconnecting arc is

then thought to be a set of reconnected loops filled by plasma, which have the same physical origin of “post” flare loops. As it is observed for some flares, the second set of reconnected field lines does not show up in the observations because its size (and in particular its volume) is too large, so that the increase in plasma density (and so in emission) is too low.

5. Conclusion

The aim of present study is to further quantify the energy release processes involved in flares. We focus here on the understanding of the link between the observed flare emissions (in $H\alpha$ and soft X-rays) and the magnetic configuration (photospheric magnetograms and coronal computed field) in two interacting active regions (ARs 7031 and 7038), observed on January 1992. Previous studies of several flares (see references in the Introduction) have shown that energy release occurs at the location of quasi-separatrice layers (QSLs) in different kinds of magnetic configurations. In this work we confirm these results with additional examples. Within the spatial resolution of the observations and the limit of the magnetic field model we have found that flare $H\alpha$ kernels and soft X-ray brightenings lie in the close vicinity of the computed QSLs (see Fig. 5). For all flares, as well as for a soft X-ray arc linking the two ARs, we are able to identify the two magnetic bipoles which interact and the magnetic connectivities before and after reconnection (see Fig. 6). Only reconnected loops are expected to be seen in the observations since pre-reconnected loops are not dense enough. During reconnection, the energy released is enough to evaporate locally the top of the chromosphere and so, the emission of the reconnected loops is strongly enhanced. We observe such pairs of X-ray loops in the three flare events. We then extend our conclusions to the plausible origin of flares and of the interconnecting arc as summarised below.

The computation of QSLs in the extrapolated field from a given magnetogram allows us to find the possible places of reconnection in the magnetic configuration as we have shown for the flares in AR 7031 (Fig. 5a–d). However, the computation of the magnetic topology at a given time cannot precise which portions of the QSLs are, or will be, involved in reconnection. These locations are indeed determined by the evolution of the magnetic configuration; that is to say, the evolution determines basically where the stronger current layers are formed and where the free magnetic energy is located. We have so far found two different kinds of magnetic field evolutions in flaring regions: emergence of new field (e.g. Mandrini et al. 1996) and photospheric horizontal displacements of magnetic polarities (e.g. Gaizauskas et al. 1998). Both cases are present in AR 7031: flux emergence for flares **A** and **A'** and photospheric flux displacements for flare **B**, respectively. The presence of a long-duration faint soft X-ray arc between AR 7031 and AR 7038 belongs to the second kind: reconnection between magnetic loops belonging to the two ARs is driven mainly by the long term rotation (of at least a week) of AR 7038. This region emerged in a North-South direction, and rotated in such a way to adopt the Hale orientation correspond-

ing to the southern hemisphere for cycle 22 (see SGD 571 Part I).

A third possibility to drive magnetic reconnection is an evolution of the magnetic configuration as a result of another nearby magnetic reconnection process. Indeed, three “sympathetic” flaring processes were observed associated to flare **B**. First, the initial energy release in flare **B** is associated to a set of QSLs (Fig. 5c, d), then it stimulates energy release in nearby QSLs: the eastern elongated ribbon extends North and the western ribbon shifts North to the nearby QSL (Fig. 5e, f). Second, flare **B** stimulated energy release at the QSLs of the morning flares (**A**, **A'**). Finally, flare **B**, which is located in the magnetic configuration of AR 7031, stimulated magnetic reconnection between the two ARs (7031 and 7038), forming a brighter soft X-ray interconnecting arc.

This study indicates also that a probable origin of observed soft X-ray interconnecting arcs between ARs can be a long-term magnetic reconnection process. AR 7038 emerged near AR 7031 in such a way that the positive polarities of both ARs were close by. As AR 7038 turned towards the Hale orientation, the magnetic connectivity between the ARs became more favourable since this implies a lower energetic field; then, the rotation of AR 7038 leads to a progressive reconnection between the magnetic configurations of the two ARs. This is the origin of the weak soft X-ray arc observed since January 24, 1992. When flare **B** occurred, it stimulated reconnection forming a brighter soft X-rays arc (see above). In the case of the arc, we were unable to find in X-rays the other reconnected loop, both because the event is weak and because such a loop is expected to be very extended; these two reasons contribute to a low plasma density, so to a low X-ray enhancement.

Then, the present analysis confirms previous results which conclude that QSLs are the places where magnetic reconnection can occur. Which of the many QSLs that are present in a configuration will be the site of magnetic reconnection depends strongly on the magnetic field evolution. In the analysed regions, three drivers are present at different locations: flux emergence, photospheric motions and sympathetic flaring. We find that the same process, magnetic reconnection, is at the origin of flaring inside one AR and of the formation of the interconnecting arc between the two ARs.

Acknowledgements. We thank T. Metcalf and S. McClymont for helpful discussions in early stages of this work. L.G.B. thanks the staff at IFA for their hospitality. Data used here from Mees Solar Observatory, University of Hawaii, are produced with the support of NASA grant NAG 5-4941 and NASA contract NAS8-40801. We thank the Yohkoh team for SXT/Yohkoh data. We acknowledge financial support from the Max Planck Institut für Extraterrestrische Physik, and from CONICET (Argentina) and NSF (USA) through the CONICET-NSF agreement. We acknowledge financial support from ECOS (France) and ANPCYT (Argentina) through their cooperative science program (A97U01).

C.H.M. and M.G.R. are members of the *Carrera del Investigador Científico*, CONICET.

References

- Alissandrakis C.E., 1981, *A&A* 100, 197
 Bagalá L.G., Mandrini C.H., Rovira M.G., et al., 1995, *Solar Phys.* 161, 103
 Chase R.C., Krieger A.S., Svestka Z., Vaiana G.S., 1976, *Space Sci. Rev.* 16, 917
 De Jager C., Svestka Z., 1985, *Solar Phys.* 100, 435
 Démoulin P., Hénoux J.C., Priest E.R., Mandrini C.H., 1996, *A&A* 308, 643
 Démoulin P., Bagalá L.G., Mandrini C.H., et al., 1997, *A&A* 325, 305
 Dennis B.R., Holman G.D., Hudson H.S., et al., 1994, *Proc. of Kofu Symposium*, NRO Report No. 360, 217
 Fárník F., Svestka Z., 1986, *Solar Phys.* 104, 321
 Fárník F., Svestka Z., Karlický M., Hudson H., 1999, *Proc. SOHO 8 Workshop, Plasma Dynamics and Diagnostics in the Solar Transition Region and Corona*. ESA SP-446, 305
 Gaizauskas, V., Mandrini, C.H., Démoulin, P., et al., 1998, *A&A* 332, 353
 Hanaoka Y., 1996, *Solar Phys.* 165, 275
 Hori K., Yokoyama T., Kosugi T., Shibata K., 1998, *ApJ* 500, 492
 Howard R., Svestka Z., 1977, *Solar Phys.* 54, 65
 Khodachenko M.L., Zaitsev V.V., 1998, *Astron. Reports* 42, 265
 Livingston W.C., Harvey J., Slaughter C., Trumbo D., 1976, *Applied Optics* 15, 40
 Liu Yang, Akioka M., Yan Y., Sato J., 1998, *Solar Phys.* 180, 377
 Mandrini, C.H., Démoulin, P., van Driel-Gesztelyi, L., et al., 1996, *Solar Phys.* 168, 115
 Mandrini C.H., Démoulin P., Bagalá L.G., et al., 1997, *Solar Phys.* 174, 229
 Manoharan P.K., van Driel-Gesztelyi L., Pick M., Démoulin P., 1996, *ApJ* 468, L73
 Mickey D.L., 1985, *Solar Phys.* 97, 223
 Ozaki M., Sato T., Hayashi T., et al., 1997, *ApJ* 481, 524
 Penn M.J., Mickey, D.L., Canfield, R.C., Labonte B.J., 1991, *Solar Phys.* 135, 163
 Pevtsov A.A., Canfield R.C., McClymont A.N., 1996, *AAS Meeting* 188, 35.03.
 Poletto G., Gary G.A., Machado M.E., 1993, *Solar Phys.* 144, 113
 Priest E.R., Forbes T., 1989, *Solar Phys.* 119, 211
 Priest E.R., Démoulin P., 1995, *JGR* 100, A12, 23443
 Rompolt B., Svestka Z., 1996, *Adv. Space Res.* 17, (4/5)115
 Sakao T., Kosugi T., Masuda S., et al., 1994, *Proc. of Kofu Symposium*, NRO Report No. 360, 169
 Schmieder, B., Aulanier, G., Démoulin, P., et al., 1997, *A&A* 325, 1213
 Svestka Z., Howard R., 1979, *Solar Phys.* 63, 297
 Svestka Z., Howard R., 1981, *Solar Phys.* 71, 349
 Tsuneta S., Acton L., Bruner M., et al., 1991, *Solar Phys.* 136, 37
 Tsuneta S., 1996, *ApJ* 456, L63
 Yoshida T., Tsuneta S., 1996, *ApJ* 459, 342